A NUMERICAL SIMULATION OF THE WOS AND THE WAVE PROPAGATION ALONG A COASTAL DIKE

Panayotis Prinos[1], Maria Tsakiri[1] and Dimitris Souliotis[1]

Wave overtopping and the propagation of the waves on the crest and the landward slope of a coastal dike is investigated numerically. Wave overtopping conditions are simulated using the concept of the Wave Overtopping Simulator (WOS). Two numerical models of the WOS are constructed using the FLUENT 6.0.12 (FLUENT Inc. 2001) and the FLOW 3D 9.4 (FLOW 3D 2010) CFD codes. The former simulates the WOS without accounting for air entrainment while the latter accounts for air entrainment. The unsteady RANS equations, the RNG k-ε turbulence model and the VOF method are solved numerically, for "tracking" the free surface and the head of the "current" from the dike crest to the landward dike slope. The computed results from the two models are compared with each other and also against field measurements and proposed empirical relationships (Van der Meer et al. 2010).

Keywords: wave overtopping simulator; coastal dike; dike crest; landward slope; air entrainment

INTRODUCTION

Coastal dikes are widely used to protect low-lying areas against floods. As such, they have been widely applied in countries such as Vietnam, Bangladesh, Thailand, the Netherlands and the USA. Dikes have been extensively utilized as flood defenses in the Netherlands over the past several hundred years as 25% of its area and 21% of its population is located below the sea level. Moreover, 800 km sea dikes are used in Vietnam in order to be protected by floods. Due to changing physical circumstances, a sea level rise is predicted and in addition to stronger storms and more wave attack, wave overtopping on the current dikes will increase. For that reason it is essential to estimate the resistant of the existing dikes and also to propose construction methods in order to increase the strength of dikes for cases which is necessary.

In order to create full scale overtopping conditions on a real landward slope of a dike the Wave Overtopping Simulator has been developed. The Wave Overtopping Simulator was first developed in the Netherlands. It is a water reservoir which is continuously filled by pumps with a certain and constant discharge of water and emptied at predefined moments through bottom valves in a way that the volumes simulate the overtopping wave tongues on the dike crest and then on the landward slope. The maximum capacity is 5500 l/m giving a total volume of 22000 l for a simulator with wide equal to 4 m. The design and the calibration of the Wave Overtopping Simulator have been described by Van der Meer (2007) and also Van der Meer et al. (2006, 2007 and 2008).

In the past years, several field experiments have been performed in order to evaluate the effect of wave overtopping on coastal dikes, using the Wave Overtopping Simulator and results have been described by Akkerman et al. (2007a and 2007b) and Steendam et al. (2008). Experimental results, using the Wave Overtopping Simulator, as well as empirical equations for flow depth and flow velocity under wave overtopping have been also presented by Van der Meer et al. (2010).

In the present work the effect of wave overtopping on the crest and the landward slope of a sea dike is studied numerically for wave volumes of 2000, 3000 and 5000 l/m. The wave overtopping conditions are created by simulating the Wave Overtopping Simulator (WOS) using two different models. The first model simulates the wave overtopping without accounting for the air entrainment while the second model takes into account air entrainment (Hirt 2003). The two models are based on the FLUENT 6.0.12 (FLUENT Inc. 2001) and the FLOW 3D 9.4 (FLOW 3D 2010) respectively. The computed results from the two models are compared with each other and also against available field experiments and empirical relationships for the prediction of maximum flow depth and velocity at various locations (Van der Meer et al. 2010).

CASES STUDIED

The dike geometry has been presented by Van der Meer et al. (2010). The length of the dike crest is 2 m at a height of 2.6 m above the ground. The landward slope is equal to 1:3.7 at the upper part, while at the lower part is equal to 1:5.2. Five measurement locations have been selected as it is shown

[1] Hydraulics Laboratory, Department of Civil Engineering, Aristotle University of Thessaloniki, Thessaloniki, 54124 Greece

in Fig. 1. The first location is at the end of the crest (Board 1), while the next four locations are along the landward slope (Board 2 to 5). Specifically Boards-2 and 3 are at the upper part (slope 1:3.7), while Boards 4 and 5 are in the region where the slope is equal to 1:5.2.

In the present study, cases with three different overtopping volumes, equal to 2000, 3000 and 5000 l/m are simulated.

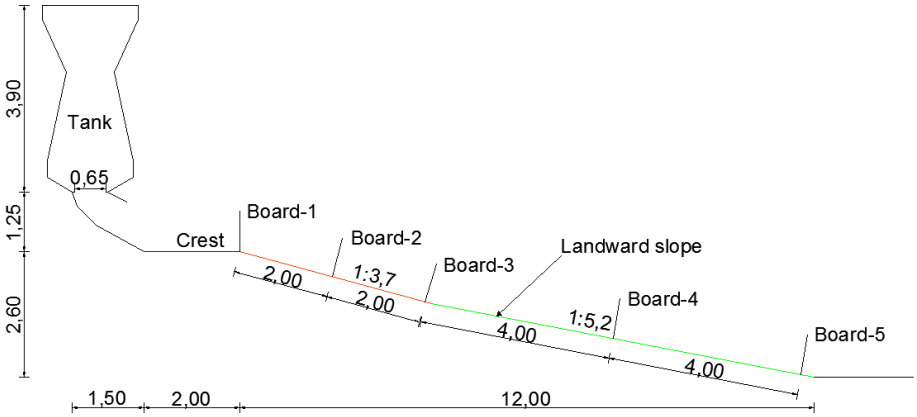

Figure 1. Wave overtopping simulator, dike geometry and measurements boards.

NUMERICAL PROCEDURE

General

In this work, two CFD codes are used for simulating the wave overtopping conditions. The first code is the FLUENT 6.0.12 (FLUENT Inc. 2001) which does not take into account the air entrainment in the flow while the second code is the FLOW 3D 9.4 (FLOW 3D 2010) which takes into account the air entrainment.

Mathematical model

The CFD codes solve the unsteady Reynolds-Averaged Navier-Stokes (RANS) equations (Eq. 1 and Eq. 2) in conjunction with the transport equations of turbulent kinetic energy k (Eq. 3) and dissipation rate ε (Eq. 4) of the RNG k-ε type turbulence model (Yakhot et al. 1992). The VOF method (Hirt and Nichols 1981) is also enabled for "tracking" the free surface from the dike crest to the toe of the landward dike slope with the volume fraction equation (Eq. 5).

$$\frac{\partial \rho_q}{\partial t} + \frac{\partial \left(\rho_q U_{i,q} \right)}{\partial x_i} = 0 \tag{1}$$

$$\frac{\partial \left(\rho_q U_{i,q} \right)}{\partial t} + U_{j,q} \frac{\partial \left(\rho_q U_{i,q} \right)}{\partial x_j} = -\frac{\partial p_q}{\partial x_i} + \frac{\partial}{\partial x_j} \left[\rho_q \left(-\overline{u_i u_j} \right)_q \right] \tag{2}$$

$$\frac{\partial \left(\rho_q k_q \right)}{\partial t} + U_{j,q} \frac{\partial \left(\rho_q k_q \right)}{\partial x_j} = \frac{\partial}{\partial x_j} \left(\frac{\mu_{t,q}}{\sigma_k} \frac{\partial k_q}{\partial x_j} \right) + \left[\rho_q \left(-\overline{u_i u_j} \right)_q \frac{\partial U_{i,q}}{\partial x_j} \right] - \rho_q \varepsilon_q \tag{3}$$

$$\frac{\partial \left(\rho_q \varepsilon_q \right)}{\partial t} + U_{j,q} \frac{\partial \left(\rho_q \varepsilon_q \right)}{\partial x_j} = \frac{\partial}{\partial x_j} \left(\frac{\mu_{t,q}}{\sigma_\varepsilon} \frac{\partial \varepsilon_q}{\partial x_j} \right) + C_{1\varepsilon} \frac{\varepsilon_q}{k_q} \left[\rho_q \left(-\overline{u_i u_j} \right)_q \frac{\partial U_{i,q}}{\partial x_j} \right] - C^*_{2\varepsilon} \rho_q \frac{\varepsilon_q^2}{k_q} \tag{4}$$

$$\frac{1}{\rho_q}\left[\frac{\partial}{\partial t}\left(\alpha_q\rho_q\right)+\frac{\partial}{\partial x_i}\left(\alpha_q\rho_q U_{i,q}\right)\right]=0 \tag{5}$$

The subscript q refers to the phase q while ρ_q is the density of each phase, α_q is the volume fraction, $U_{i,q}$ is the velocity in the i direction, p_q is the effective pressure (the difference between the static and the hydrostatic pressure), $\left(-\overline{u_i u_j}\right)_q$ are the turbulent stresses , $\mu_{t,q}$ is the eddy viscosity , σ_k, σ_ε, $C_{1\varepsilon}$ and $C_{2\varepsilon}$ are coefficients, $\rho_q\left(-\overline{u_i u_j}\right)_q\frac{\partial U_{i,q}}{\partial x_j}$ is the production of turbulent kinetic energy and $C^*_{2\varepsilon}$ is given by the equation:

$$C^*_{2\varepsilon}=C_{2\varepsilon}+\frac{C_\mu\eta^3\left(1-\eta/\eta_0\right)}{1+\beta\eta^3} \tag{6}$$

where $\eta=Sk/\varepsilon$ (S is the rate of strain tensor), C_μ, $C_{2\varepsilon}$, η_0 and β are coefficients.

Initial conditions

The FLUENT CFD code (FLUENT Inc. 2001) uses a control-volume technique in order to convert the governing equations to algebraic equations which can be solved numerically. For the construction of the grids the GAMBIT program is used. The grids are two-dimensional, structured and the shape of the cells is orthogonal. The number of computational cells for the cases which are studied is equal to 200000. The initial values of turbulent kinetic energy and dissipation rate are equal to 10^{-4} and 10^{-5} respectively. The simulations are time-dependent and the time step which is used is equal to $5x10^{-4}$ s.

The FLOW 3D CFD code (FLOW 3D 2010) is applied in order to convert the governing equations to algebraic equations. For the geometric construction of the model the AutoCAD program is used while the mesh is constructed with the FLOW 3D. The grids are two-dimensional, structured and the shape of the cells is orthogonal. The number of computational cells varies between 300000 and 600000 for the cases studied. In order to simulate air entrainment, the second option of air entrainment model is used which is based on a variable density formulation (Hirt 2003). This model includes the "bulking" of fluid volume by the addition of air and the buoyancy effects associated with entrained air. Two coefficients should be set, the air entrainment rate coefficient is set 0.5 and the surface rate coefficient is set 0.073.

Solving procedure

Initially, water is present in the tank while air is in the rest of the computational domain (Fig. 2 and Fig. 3). The water flows through the exit of the tank due to gravity. The RANS equations and the transport equations of turbulent kinetic energy and dissipation rate are non-linear and coupled which means that during a time step several iterations of the solution loop are performed before a converged solution is obtained. The volume fraction equation is also solved, with regard to the VOF method, once for each time step.

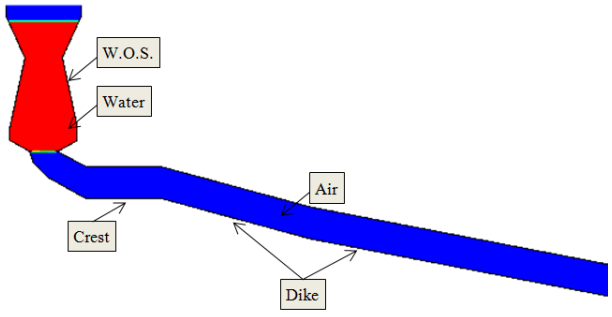

Figure 2. Computational domain for the FLUENT CFD code.

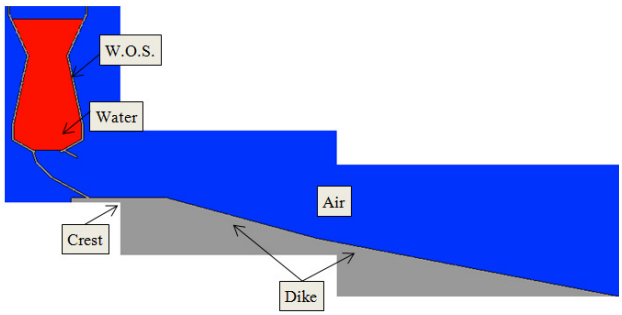

Figure 3. Computational domain for the FLOW 3D CFD code.

ANALYSIS OF THE RESULTS

Fig. 4 shows the variation of the computed flow depth with time, for water volume of the simulator equal to 2000 l/m, at four different locations (Board 1,2,3 and 5). In the same figure the variation of the experimental flow depth with time is shown for three different waves (Exp. Data 1-3) with the same volume, at the same locations. It is observed that the flow depth increases suddenly in the beginning as the wave passes from a particular location. The maximum flow depth is higher at Board 1 than that at the other Boards which means that it decreases as the wave travels along the landward slope of the dike. Moreover the maximum computed flow depth is in good agreement with the maximum experimental flow depth at Board 1 and 5 but it is higher at the other two Boards. However, the duration of the experimental maximum flow depth is higher than that of the numerical simulations. Moreover the computed results increase at Boards 3 and 5 faster than the experimental results which means that the numerical waves travel faster.

In Fig. 5 the variation of computed the flow depth with time is shown at the same locations (Board 1,2,3 and 5) together with the variation of the experimental flow depth, from three waves, for 3000 l/m water volume. The maximum computed flow depth is in satisfactory agreement with the maximum experimental flow depth. Flow depth computed by Flow 3D CFD code (model with air entrainment) is a little higher than that of Fluent CFD code simulation (model without air entrainment).

Fig. 6 shows the variation of the computed flow depth with time at four locations (Board 1,2,3 and 5) together with the variation of the experimental flow depth, from three waves, for 5000 l/m water volume. The maximum computed flow depth by Flow 3D is in good agreement with the maximum experimental flow depth with the exception of this at Board 2 where experimental flow depth is much higher.

In Fig. 7 the variation of the computed flow velocity with time is shown at the Boards 1, 2, 3 and 5, for water volume equal to 2000 l/m. Experimental results for the three waves are available only at Board 5. The flow velocity increases suddenly in the beginning as the wave passes from a particular location. The computed flow velocity by the Flow 3D is lower than this computed by Fluent and it is in quite good agreement with experimental results at Board 5.

Fig. 8 shows the variation of the computed flow velocity with time at the same locations (3000 l/m water volume). Available experimental results are also shown in the same figure, for the same water volume. It is observed that the maximum computed velocity by the Flow 3D is approximately the same at all the locations studied. Moreover at Board 3 computed velocities are much higher than experimental velocities, but at Board 5 velocities by Flow 3D are in quite good agreement with these which arises from the experiments.

In Fig. 9 the variation of the computed flow velocity with time is shown at the Boards 1,2,3 and 5, for water volume equal to 5000 l/m, together with available experimental results where they are available. The flow velocity which is computed by Flow 3d is lower than that computed by Fluent. Moreover the flow velocity computed by Flow 3D is quite higher than the experimental flow velocity at Board 3 but it is in good agreement with it at the Board 5.

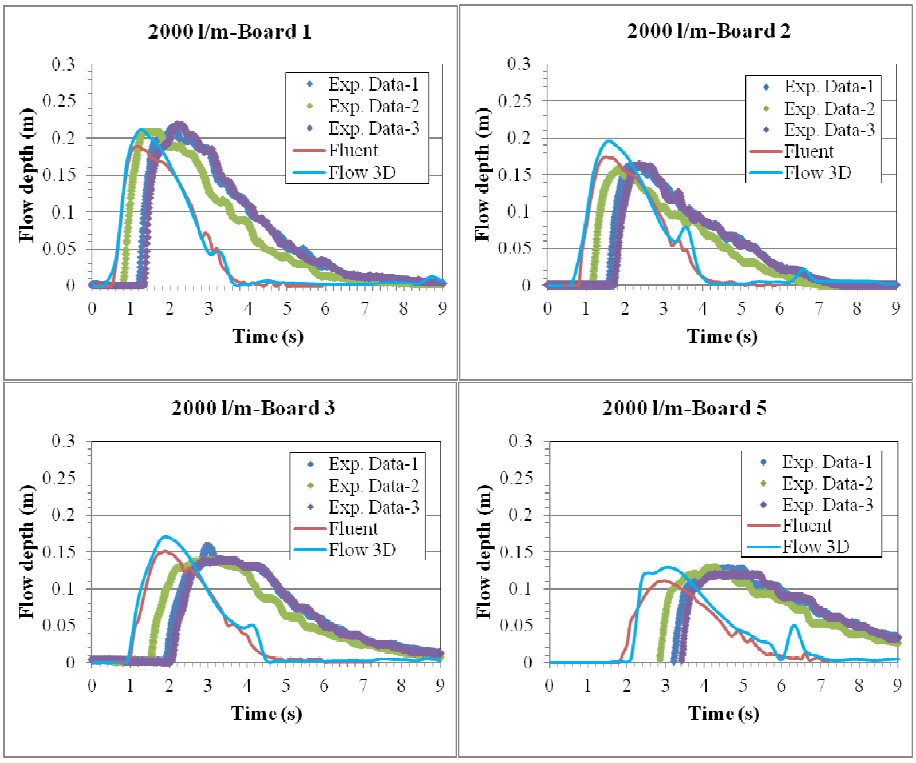

Figure 4. Variation of flow depth with time (water volume 2000 l/m).

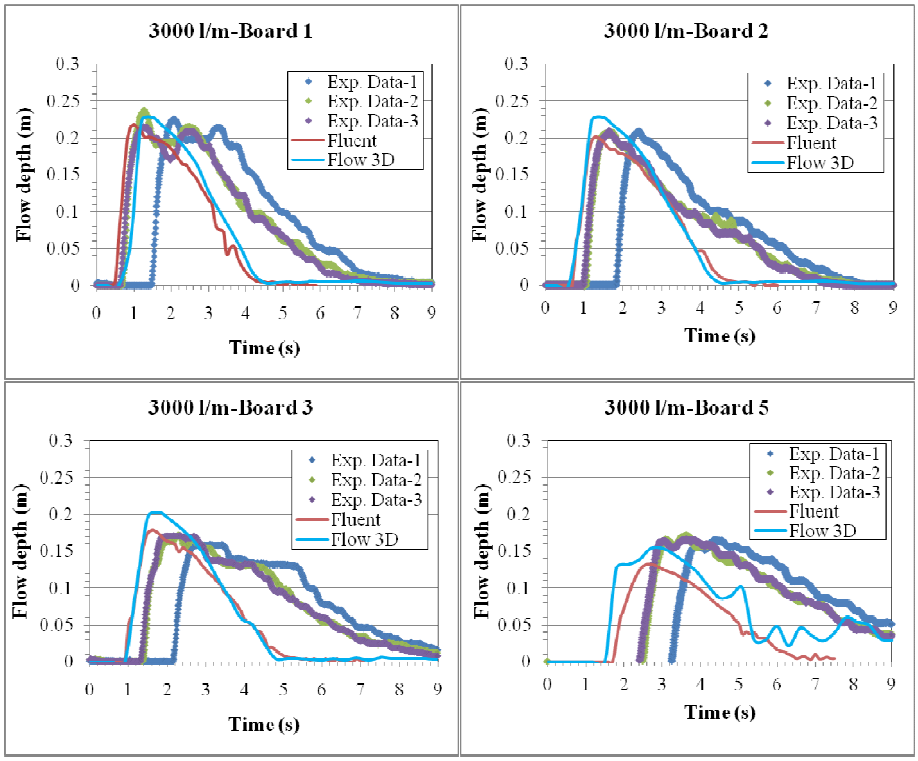

Figure 5. Variation of flow depth with time (water volume 3000 l/m).

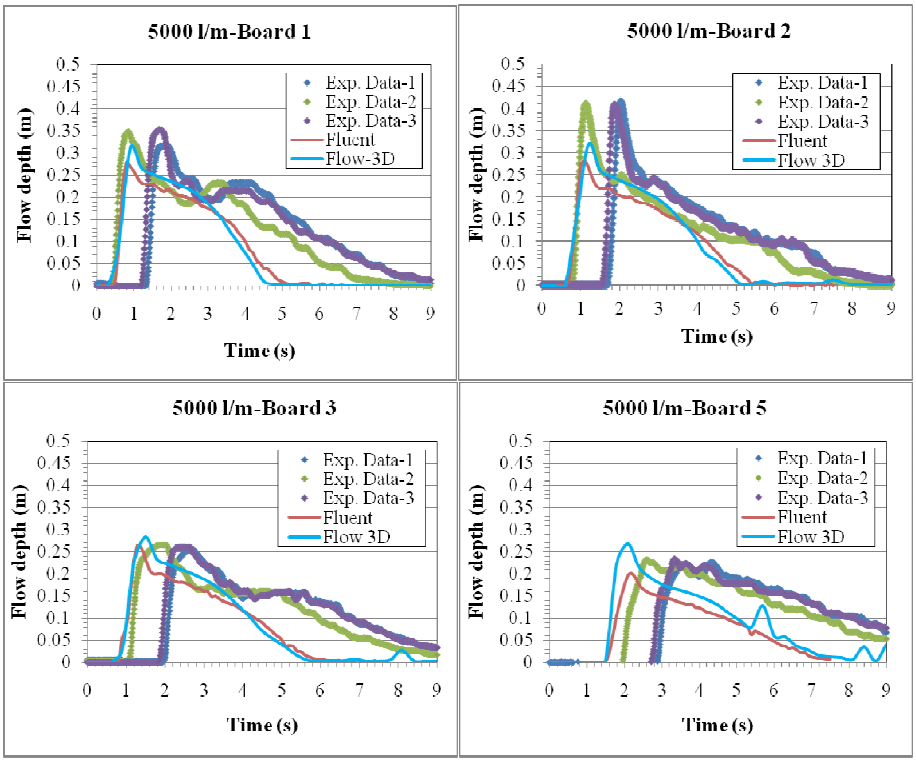

Figure 6. Variation of flow depth with time (water volume 5000 l/m).

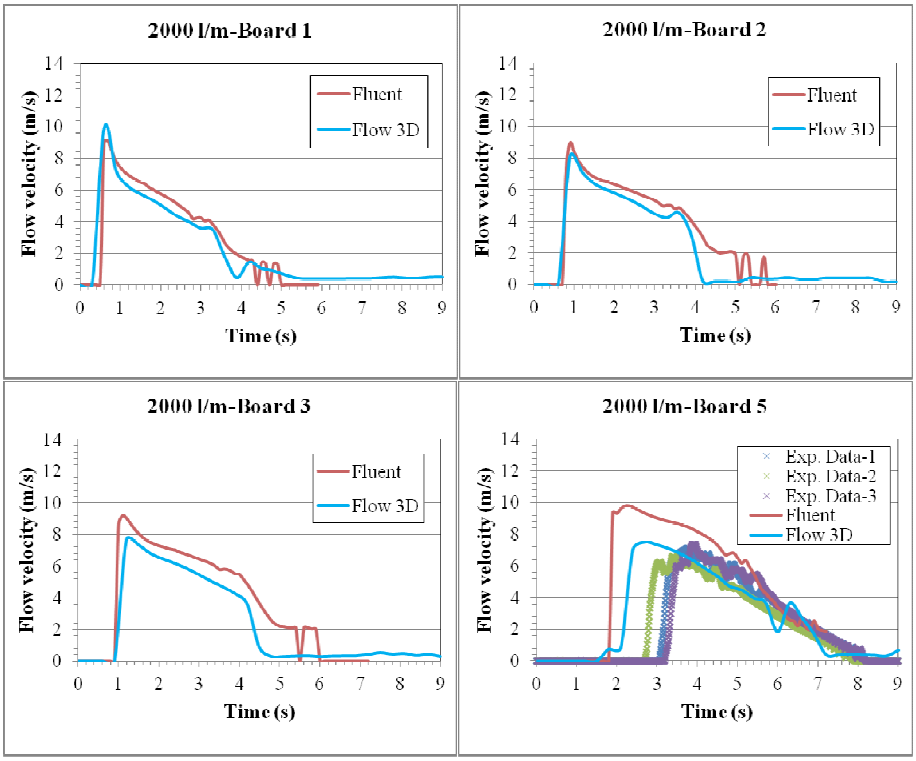

Figure 7. Variation of flow velocity with time for water volume 2000 l/m at four different locations.

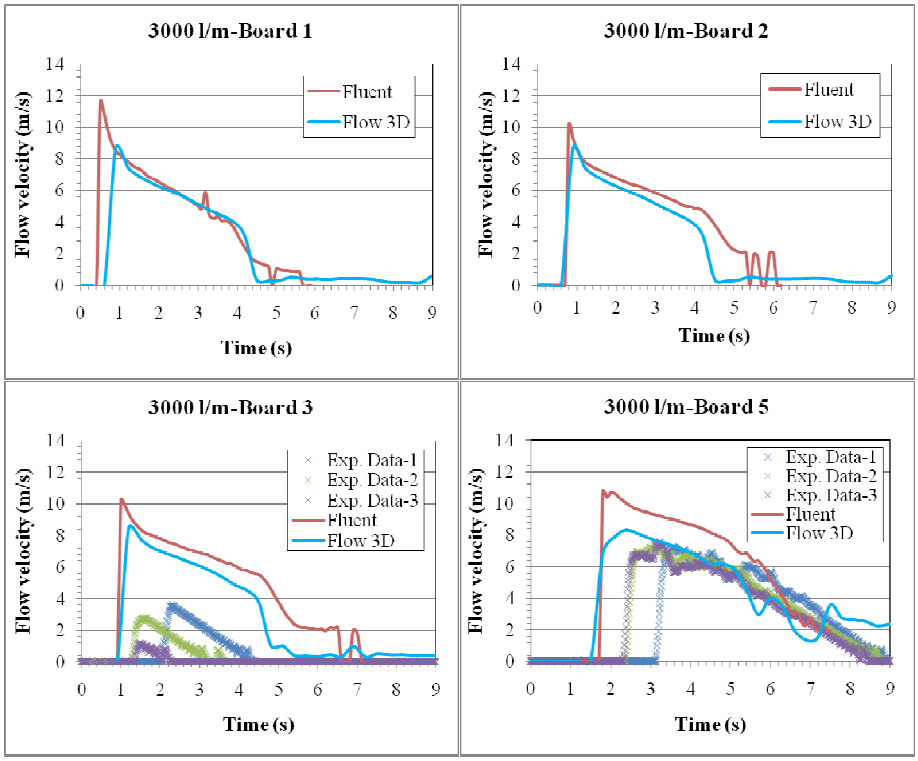

Figure 8. Variation of flow velocity with time (water volume 3000 l/m).

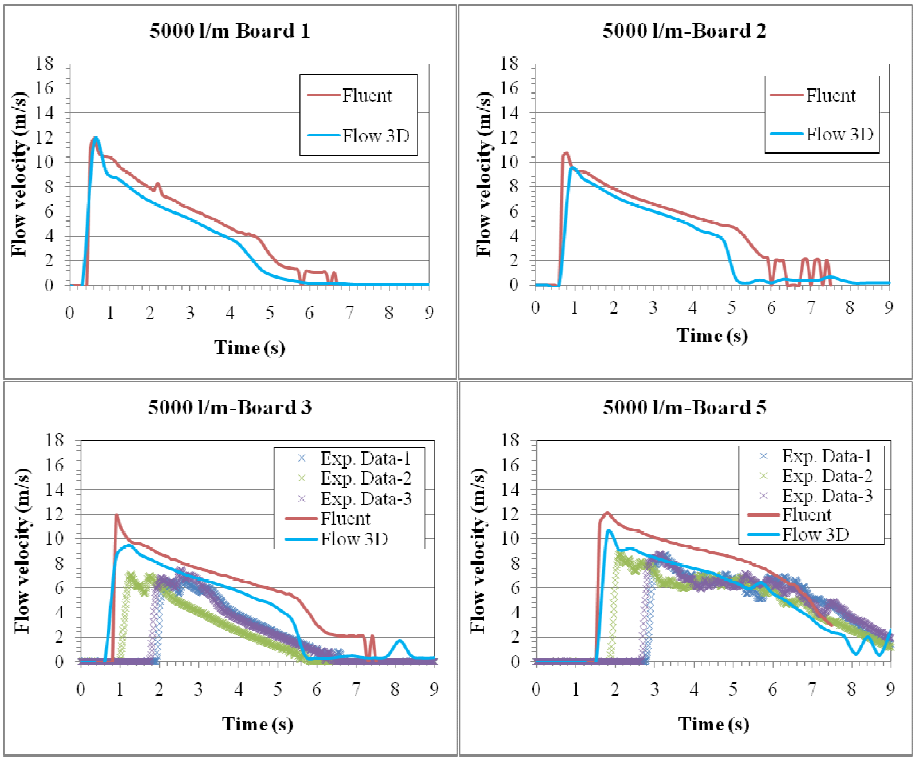

Figure 9. Variation of flow velocity with time (water volume 5000 l/m).

In Fig. 10 the variation of the computed maximum flow depth and velocity with the overtopping wave volume is shown together with an empirical relationship, based on field measurements with the wave overtopping simulator, proposed by Van der Meer et al. (2010). The agreement between the computed maximum flow depth and that predicted by the expression $h=0.133V^{0.5}$ (h= flow depth (m) and V= water volume (m^3/m)) is quite satisfactory for the Board 1 (dike crest) and Board 2 while the flow depth at the other Boards in the landward slope of the dike is lower. Similar behavior is indicated by the measured flow depths of Van der Meer et al. (2010). The computed maximum velocities are shown to be increased with regard to those of the proposed relationship $u=0.5V^{0.34}$ (u= flow velocity (m/s)), however the results from the model with air entrainment (Flow 3D) are better than those of the model without air entrainment (Fluent). The difficulty in measuring the maximum velocity in the field as well as the difficulty of simulating the air entrainment in the computations may contribute to such discrepancies.

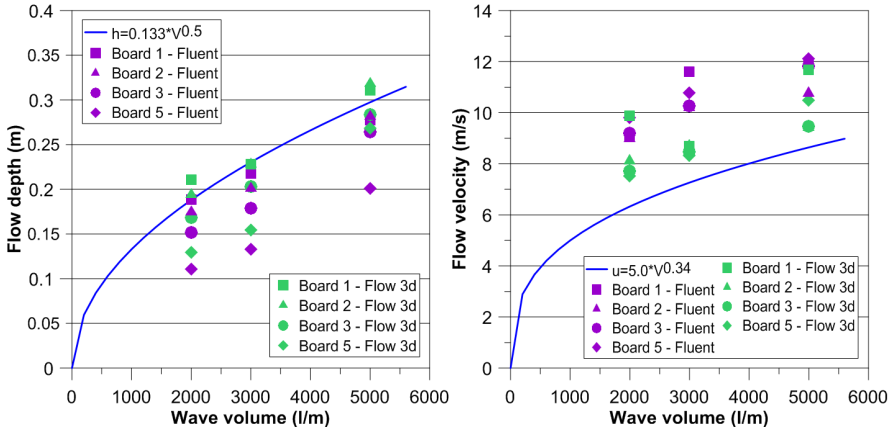

Figure 10. Variation of maximum flow depth and velocity with wave volume.

CONCLUSIONS

Wave overtopping and the propagation of the waves on the crest and the landward slope of a coastal dike is investigated numerically. Wave overtopping conditions are simulated using the concept of the Wave Overtopping Simulator. The unsteady RANS equations in conjunction with a turbulence model of the RNG k-ε type and the VOF method are solved numerically, for "tracking" the free surface and the head of the "current" from the dike crest to the toe of the landward dike slope. Computed results of two models (with and without air entrainment) are compared with each other and also against proposed empirical relationships based on available field measurements of Van der Meer et al. (2010) and experimental data. The following conclusions can be derived:

- Maximum computed flow depth is in agreement with maximum experimental flow depth. It is also in quite good agreement at Board-1 with the empirical relationship presented by Van der Meer et al. (2010).
- Computed velocities by Fluent (model without air entrainment) are higher than those of the Flow 3D (model with air entrainment). Moreover they are higher than experimental velocities and the velocities from the empirical relationship (Van der Meer et al. 2010). However, the difficulty in measuring the maximum velocity in the field as well as the omission of the air entrainment in the computations (model without air entrainment - Fluent) make such a comparison to be considered with caution.
- Computed velocities by Flow 3D (model with air entrainment) are in better agreement with experimental velocities and also with the velocities which arise from the empirical relationship (Van der Meer et al. 2010).
- The higher the initial volume of the water the better the agreement between computed results and experimental data.

ACKNOWLEDGMENTS

The support of the European Commission through FP7.2009-1, Contract 244104 - THESEUS ("Innovative technologies for safer European coasts in a changing climate"), is gratefully acknowledged.

REFERENCES

Akkerman, G.J., Bernadini, P., Van der Meer, J.W., and Van Hoven, A. 2007a. Field tests on sea defences subject to wave overtopping, *Proceedings of Coastal structures*, ASCE, Venice, Italy, 657-668.

Akkerman, G.J., Van Gerven, K.A.J., Schaap, H.A. and Van der Meer, J.W. 2007b. Wave overtopping erosion tests at Groningen sea dyke, *ComCoast*, Workpackage 3: Development of Alternative Overtopping-Resistant Sea Defences, phase 3. (www.comcoast.org).

ANSYS. Fluent Inc. 2001. Fluent 6.0 Documentation, Lebanon, USA.

FLOW 3D. 2010. User Manual Version 9.4, Flow Science, Inc., Santa Fe.

Hirt C.W. 2003. Modeling turbulent entrainment of air at a free surface, Technical note 61, Flow Science, Inc. (FSi-03-TN61).

Hirt C.W., Nichols B.D. 1981. Volume of fluid (VOF) method for the dynamics of free boundaries, *Journal of Computational Physics,* 39, 201-225.

Steendam, G., De Vries, W., Van der Meer, J.W., Van Hoven, A, De Raat, G. And Frissel, J.Y. 2008. Influence of management and maintenance on erosive impact of wave overtopping on grass covered slopes of dikes, *Proceedings of Flood Risk Management: Research and Practice*, Oxford, UK, 95 pp. (full paper available in CD-ROM).

Van der Meer, J.W., Snijders, W. and Regegling, E. 2006. The wave overtopping simulator, *Proceedings of ICCE 2006*, ASCE, San Diego, USA, 4654-4666.

Van der Meer, J.W. 2007. Design, contruction, calibration and use of the wave overtopping simulator. *ComCoast*, Workpackage 3: Decelopment of Alternstive Overtopping-Resistant Sea Defences, phase 3. (www.comcoast.org.)

Van der Meer, J.W., Bernadini, P., Akkerman, G.J. and Hoffmans, G.J.C.M. 2007. The wave overtopping simulator in action, *Proceedings of Coastal Structures*, ASCE, Venice, Italy, 645-656.

Van der Meer, J.W., Steendam, G., de Raat and Bernadini, P. 2008. Further developments on the wave overtopping simulator, *Proceeding of ICCE 2008*, ASCE, Hamburg, Germany, 2957-2969.

Van der Meer, J.W., Hardeman, B., Steendam, G., Schuttrumpf, H. And Verheij, H. 2010. Flow depths and velocities at crest and inner slope of a dike, in theory and with the wave overtopping simulator, *Proceedings of ICCE 2010*, Shanghai, China.

Yakhot, V., Orszag, S.A., Thangam, S., Gatski, T.B. and Speziale, C.G. 1992. Development of turbulence models for shear flows by a double expansion technique, *Physics of Fluids A,* 4, 1510-1520.